Tensile properties of high- and medium-entropy alloys

A. Gali [a,b], E.P. George [a,b,*]

[a] Materials Science and Technology Division, Oak Ridge National Laboratory, Oak Ridge, TN 37831, USA
[b] Department of Materials Science and Engineering, University of Tennessee, Knoxville, TN 37996, USA

A B S T R A C T

Equiatomic, face-centered-cubic, high- and medium-entropy alloys were arc melted, hot-rolled to produce recrystallized sheets, and tensile tested. The alloys having the compositions CrMnFeCoNi and CrFeCoNi exhibited a strong temperature-dependent decrease in strength with increasing temperature from $-196\ ^\circ$C to 1000 $^\circ$C, and a relatively weak strain-rate dependence (at 10^{-3} and 10^{-1} s^{-1}). Ductility did not vary inversely with yield strength; rather, when strength doubled as the test temperature was decreased from room temperature to $-196\ ^\circ$C, elongation to fracture increased by a factor of 1.5 to >60%. A high degree of work hardening, possibly due to deformation-induced nanotwinning, postpones the onset of necking and may be the reason for the ductility increase.

© 2013 Elsevier Ltd. All rights reserved.

1. Introduction

Recently, there has been considerable interest in multi-element, equiatomic alloys and their derivatives e.g.[1–20], that are often referred to in the literature as high-entropy alloys. In ideal solid solutions, the configurational entropy, $\Delta S_{conf} = -R\Sigma n_i ln(n_i)$, where n_i is the atomic fraction of the ith element and R is the gas constant, increases with the number of alloying elements. It has been hypothesized that, when the number of alloying elements increases beyond five, the contribution of configurational entropy to the total free energy becomes significant enough that it can overcome the enthalpies of compound formation and phase separation, thereby stabilizing the solid solution state relative to multi-phase microstructures [1]. Based on this logic, a high-entropy alloy was defined as one with at least five major elements whose individual atomic concentrations are between 5 and 35% [1,7]. Alloys based on one principal metallic element were classified as low-entropy alloys and those comprised of two to four principal elements as medium-entropy alloys [7]. In all such multi-element alloys, the configurational entropy is obviously maximized when the alloying elements are present in equal atomic concentrations [1]; consequently, much of the high-entropy alloy research has tended to focus on alloys consisting of multiple principal elements in roughly equal proportions.

While the above concepts can, in principle, explain why *some* multi-element alloys are single-phase solid solutions [2,13,14,16,17,19,20], most of the so-called high-entropy alloys reported in the literature contain multiple phases [e.g.,4-12,15]. The reason for this is that configurational entropy cannot usually overcome the other driving forces of phase stability, such as enthalpy and non-configurational entropy, which often have stronger influences [19]. Additionally, in alloys consisting of multiple phases, the configurational entropy is actually lower than that implied by the equation above for a single-phase ideal solid solution [19]. Therefore, to study the mechanical properties of *high-entropy* alloys, it is important that truly single-phase solid solution alloys be investigated.

Here we investigate the equiatomic, FCC-structured quinary alloy (CrMnFeCoNi), first reported by Cantor et al.[2] and later confirmed to consist of a single solid-solution phase [19,20]. For comparison with this high-entropy alloy, we investigated a medium-entropy quaternary alloy (CrFeCoNi) that is comprised of the same elements as the Cantor alloy minus the Mn; this quaternary alloy is also single-phase FCC [17]. The tensile properties of neither of these alloys have so far been published. We report here our initial findings on the microstructure and tensile behavior of these alloys, which were produced by arc melting, drop casting and hot rolling, as described below.

2. Materials and methods

Starting from the pure (>99.9% purity) constituent elements in bulk form, two alloys having the equiatomic compositions CrMnFeCoNi (HE-1) and CrFeCoNi (HE-4) were produced by arc

* Corresponding author. Materials Science and Technology Division, Oak Ridge National Laboratory, Oak Ridge, TN 37831, USA. Tel.: +1 865 574 5085.
E-mail address: georgeep@ornl.gov (E.P. George).

melting under argon atmosphere. The arc-melted buttons were flipped and remelted five times to promote thorough mixing and to allow the regions in contact with the water-cooled copper hearth to become fully incorporated in the melt. After the fifth remelt, the arc-melted buttons were drop cast into a rectangular copper mold measuring 127 mm × 25.4 mm × 12.7 mm. Weight losses after melting and casting were ∼1% and <0.1% for the HE-1 and HE-4 alloys, respectively. Since there was negligible weight loss in the alloy without Mn, it was assumed that the entire weight loss in HE-1 was due to evaporation of Mn (consistent with its much higher vapor pressure). To compensate for this weight loss, we added an extra gram of Mn per 100 g of raw materials.

The drop-cast bars exhibited dendritic segregation; therefore, they were first annealed at 1000 °C for 24 h in vacuum to homogenize their compositions. After homogenization, the alloys were clad with stainless steel sheet and hot rolled to break down their cast structures and obtain a recrystallized microstructure. The purpose of the cladding was to minimize heat loss to the unheated rolls during the rolling operation. Before the first rolling pass, the clad bars were pre-heated at 1000 °C for 1 h; between all subsequent passes, reheating to 1000 °C was done for ∼15 min. For the first five rolling passes, a 10% reduction in thickness per pass was used; after that, a 20% reduction in thickness per pass was used for all subsequent passes until a final sheet thickness of ∼1 mm was reached. Therefore, starting from the initial thickness of the drop-cast bar (12.7 mm), the total reduction in thickness after rolling was ∼92%.

To evaluate the microstructures of the alloys, transverse sections were cut by electric discharge machining (EDM) from the homogenized bars and hot-rolled sheets. The sections were mounted in epoxy, ground through 600 grit SiC paper, and polished using Vibromet machines, first with 0.3 μm Al_2O_3 and then in a suspension of colloidal silica having a particle size of 60 nm. The polished samples were examined in an XL30 FEG scanning electron microscope (SEM) in the backscattered electron mode. Specimens from the homogenized bars were also used to (a) obtain x-ray diffraction patterns in a Scintag diffractometer and (b) determine their melting points in a NETZSCH 404 C differential scanning calorimeter.

From the rolled sheets, dog-bone shaped specimens with gage sections of 10 mm × 2.5 mm × 0.63 mm were cut by EDM with their long axes parallel to the rolling direction. They were subsequently ground through 1200 grit SiC paper, and stress relieved at 900 °C for 1 h in vacuum. Tensile tests were performed on a screw-driven Instron machine at engineering strain rates of approximately 10^{-3} and 10^{-1} s^{-1} at temperatures from −196 °C to 1000 °C. The cryogenic tests were performed with the specimens completely immersed in liquid nitrogen; tests at room temperature and higher were performed in vacuum. Prior to testing, seven, roughly equally spaced Vickers indents were made on the gage sections using a micro-hardness tester and a 300-g load. The distance between adjacent indents was measured before and after the tensile tests and averaged for each specimen to get the uniform elongation to fracture (the two indents on either side of the fracture plane were excluded from the measurements). Occasionally, all the indents could not be located after testing; in those cases, the total change in specimen length divided by the gage length was used as a measure of ductility (implicitly assuming that all the deformation occurred in the gage section). Fracture surfaces of the tensile tested specimens were examined either in an XL30 or Hitachi S4800 FEG scanning electron microscope.

3. Results and discussion

Backscattered electron images of the cast and homogenized microstructures are shown in Fig. 1 (a) and (b). Both alloys are essentially single-phase; however, HE-1 contains isolated dark particles that are not present in the HE-4 alloy. Energy dispersive X-ray spectroscopy was performed on these particles. Oxygen, chromium and manganese peaks were detected, which leads to the conclusion that the particles are oxides. Since they were absent in the Mn-free HE-4 alloy, the oxygen contamination is likely associated with the Mn, but whether it was introduced through the raw
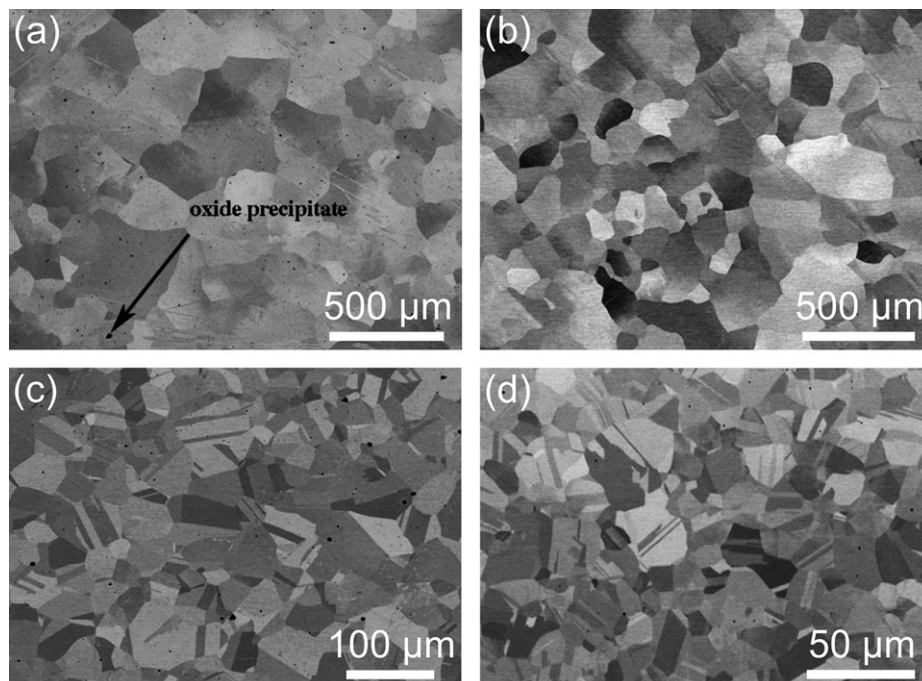

Fig. 1. Backscattered electron images of (a) CrMnFeCoNi (HE-1), (b) CrFeCoNi (HE-4) after casting and homogenization, and (c) CrMnFeCoNi (HE-1), (d) CrFeCoNi (HE-4) after hot rolling.

materials or during one of the subsequent processing steps is not known. Regardless, because of their tiny volume fraction, they did not significantly influence mechanical properties as shown below.

X-ray diffraction patterns were obtained from the two alloys in the homogenized condition. All the peaks could be indexed as FCC. There were no peaks corresponding to the oxide particles in HE-1, consistent with their low volume fraction. The melting point ranges, as determined by differential scanning calorimetry, were determined to be 1280–1349 °C and 1422–1462 °C, for the HE-1 and HE-4 alloys, respectively, indicating that the addition of Mn to the quaternary depresses the melting point and increases the gap between the solidus and liquidus.

Fig. 1 (c) and (d) show the microstructures of the two alloys after hot rolling. The microstructures are fully recrystallized indicating that dynamic recrystallization occurred during the hot rolling. Grain sizes of the roughly equiaxed grains were measured using the linear intercept method on a plane perpendicular to the rolling direction in the through-thickness (short-transverse) direction and found to be approximately 32 μm and 11 μm for the HE-1 and HE-4 alloys, respectively. The larger grain size of the HE-1 alloy may be at least partly due to the higher homologous temperature ($\sim 0.81\ T_m$) at which it was hot rolled compared to the HE-4 alloy ($\sim 0.75\ T_m$). Grain sizes were also measured after the rolled sheets were annealed for 1 h at temperatures of 600–1000 °C. No change in grain size was observed up to 800 °C; only at temperatures of 900 °C and higher was grain growth observed. These results are consistent with the notion that the alloys recrystallized during the hot rolling operation. To relieve any residual stresses in the rolled sheets, they were annealed for 1 h at 900 °C prior to tensile testing. The grain sizes after this stress-relief heat treatment were approximately 35 and 14 μm for the HE-1 and HE-4 alloys, respectively (slightly larger than in the as-rolled state, 32 and 11 μm).

Numerous annealing twins are visible in both alloys after recrystallization [Fig. 1 (c) and (d)]. Since annealing twins are commonly found in recrystallized FCC metals and solid solution alloys with relatively low stacking fault energies [21], it is reasonable to conclude that our HE-1 and HE-4 alloys have low stacking fault energies.

Fig. 2 (a) and (b) show the temperature dependencies of the 0.2% offset yield strengths of HE-1 and HE-4 tensile tested at strain rates of 10^{-3} and $10^{-1}\ s^{-1}$, respectively. The two alloys show broadly similar behavior over the ranges investigated: strong temperature dependence and weak strain-rate dependence. The temperature dependence is strongest at low and high temperatures with a smaller slope in between. Both alloys exhibit somewhat higher strengths at the higher strain rate, especially at temperatures below ~ 600 °C. At intermediate temperatures, the slope is less steep at the slower strain rate, but in neither case does yielding appear to be truly athermal, although additional experiments at intermediate temperatures are warranted to obtain better statistics. The larger grain size of HE-1 relative to HE-4 (35 vs. 14 μm) appears not to have a significant effect.

The above temperature dependence of yield strength is not usually observed in pure FCC metals; however, it is known to occur in binary solid-solution alloys [22–29]. In pure FCC metals, the athermal portion of the yield stress versus temperature curve is large compared to the thermal part, unlike in BCC metals where the opposite is the case. Since the athermal region is where thermal activation can overcome barriers to dislocation motion, these barriers are believed to be weak in pure FCC metals and easily overcome by thermal fluctuations even at cryogenic temperatures. Solute atoms can increase significantly the thermal part of the yield stress, as seen in Fig. 2 for the quinary and quaternary alloys, and reported earlier for binary FCC alloys. Thus, solute atoms introduce obstacles to dislocation motion that are not as easily overcome by thermal activation. However, the nature and strength of these obstacles may be different in relatively dilute binaries compared to the equiatomic quinary/quaternary alloys investigated here. In binary FCC alloys, the transition between the thermal and athermal regions often occurs at relatively low temperatures, e.g., at around room temperature in Cu–Zn binaries [23], which implies barrier strengths on the order of kT at room temperature, namely, 0.025 eV. By contrast, the thermal regions in Fig. 2 extend to significantly higher temperatures, implying the presence of relatively strong obstacles in our HE-1 and HE-4 alloys. Some of this difference may be due to the shorter distance between atoms of different kinds in multi-element equiatomic alloys compared to more dilute solid solutions. That is, as dislocations move in the HE-1 and HE-4 alloys, they encounter obstacles over lengths scales that are fractions of a unit cell in dimension (as opposed to distances of a few unit cells in more dilute alloys). In addition, the disparate alloying elements in HE-1 and HE-4, although they are substitutional in nature, could possibly introduce tetragonal distortions that offer more resistance
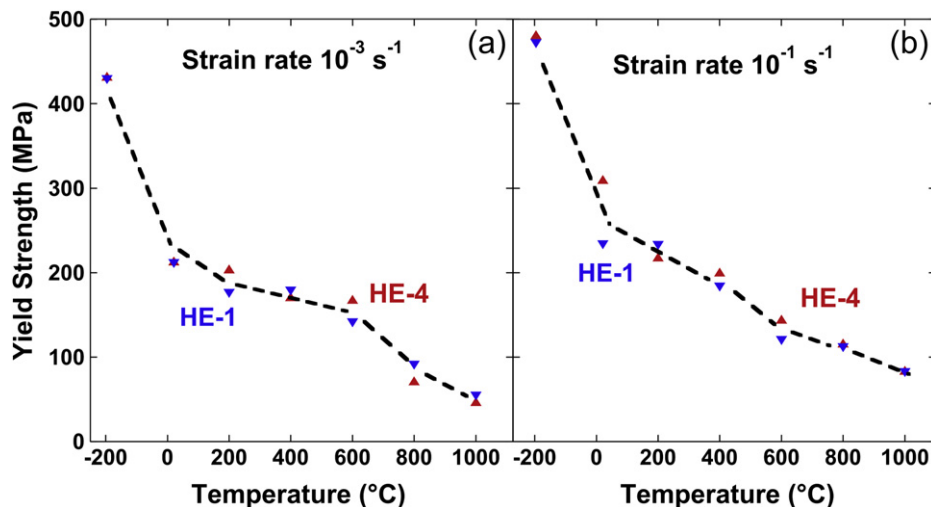

Fig. 2. Temperature dependencies of the 0.2% offset yield strengths of the CrMnFeCoNi (HE-1) and CrFeCoNi (HE-4) alloys tensile tested at engineering strain rates of $10^{-3}\ s^{-1}$ (a), and $10^{-1}\ s^{-1}$ (b).
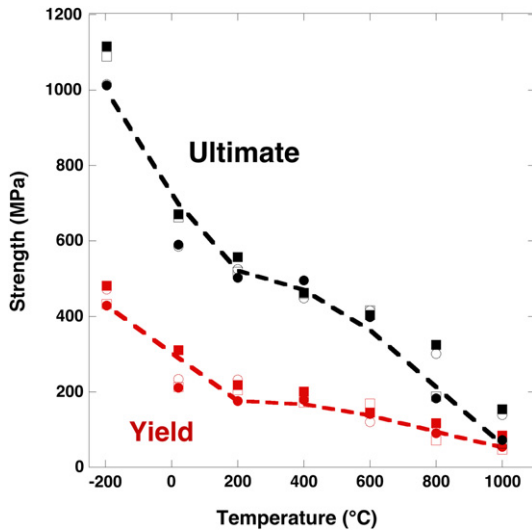
Fig. 3. Comparison of the temperature dependencies of the ultimate tensile strength and yield strength for the two alloys and strain rates investigated in this study. The circles represent the HE-1 alloy and the squares the HE-4 alloy; for each, the filled symbols are for 10^{-3} s^{-1} strain rate and the open symbols for 10^{-1} s^{-1}. To first order, the small variations between the two alloys and strain rates are ignored, so only one dashed curve is drawn (as a guide to the eye) through each data set.

to dislocation motion [30]. Clearly, further investigations are needed to understand the nature of these obstacles and how they might be different in the binary and higher-order alloys.

Fig. 3 compares the ultimate tensile strengths of the two alloys with their yield strengths. The dashed lines through the data points are merely visual aids; for the sake of simplicity, we have drawn only one line each through all of the yield and ultimate strengths (implicitly ignoring any differences between the two alloys and strain rates). There is significant work hardening at low temperatures as evidenced by the large difference between the yield and ultimate strengths (this is clearly seen on the stress–strain curves which are not shown here). While both the yield and ultimate strengths show strong temperature dependence, the latter decreases more rapidly with increasing temperature. This is

consistent with the decreasing work hardening rates with increasing temperature seen on the stress–strain curves.

Fig. 4 (a) shows the tensile ductilities of HE-1 and HE-4 as a function of temperature for an engineering strain rate of 10^{-3} s^{-1}. Surprisingly, ductility does not show an inverse dependence on strength; rather, both strength [Fig. 2 (a) and (b)] and ductility [Fig. 4(a)] increase with decreasing temperature. Between room temperature and liquid nitrogen temperature, as the yield strength doubles, the elongation to fracture increases by a factor of 1.5 (to values in excess of 60%). As can be seen in the low-magnification fractograph on the left [Fig. 4 (b)], the fracture surface of HE-4 tested at −196 °C exhibits almost no necking (HE-1 showed similar behavior). This, combined with the high work hardening implicit in Fig. 3, suggests that the large elongations at cryogenic temperatures are the result of the necking instability being postponed to higher strains. When fracture finally occurs, it is by dimpled rupture (ductile transgranular) as shown in the higher magnification fractograph on the left [Fig. 4 (c)]. At elevated temperatures, the fracture mode is again dimpled rupture [Fig. 4 (d)] but the fracture surface exhibits significant necking [Fig. 4 (e)]. The lower ductilities at elevated temperatures are likely the result of an earlier onset of the necking instability, which in turn is related to the lower work hardening seen at elevated temperatures (Fig. 3).

A possible reason for the high degree of work hardening at low temperatures is deformation-induced twinning. Nanoscale twins were recently observed in TEM specimens prepared from another batch of the HE-1 alloy tensile tested at −196 °C to a strain of ∼20% [31]. While slip is the usual deformation mode in most FCC metals, twinning can occur at low temperatures in low-stacking-fault-energy metals and is sometimes associated with serrations on the stress–strain curves [32]. For a given temperature and strain rate, the magnitude of the serrations depends on stacking-fault energy [33]: the lower its value the smaller the serrations. In our alloys, the stress–strain curves did not exhibit any serrations at room temperature or below. This could be because our specimens were polycrystalline (so twinning might occur in multiple grains simultaneously making load-drops harder to detect) or the stacking-fault energies of our alloys are low enough to make the serrations disappear. Additional work is needed to distinguish between these two possibilities.
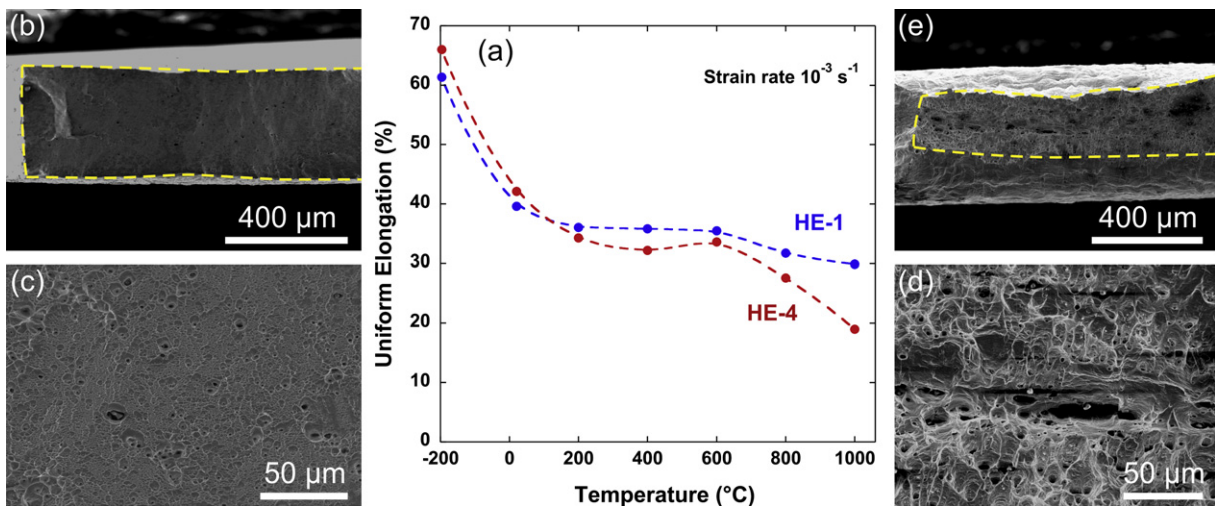

Fig. 4. (a) Temperature dependence of the tensile ductilities of CrMnFeCoNi (HE-1) and CrFeCoNi (HE-4) tested at an engineering strain rate of 10^{-3} s^{-1}. Also shown are fractographs of specimens tested at −196 °C (b, c) and 400 °C (d, e). The dashed outlines of the fracture surfaces show that there is less thickness reduction (necking) at −196 °C (b) than at 400 °C (e).

4. Summary and conclusions

Two equiatomic, multi-element alloys were produced by arc melting and hot rolling. The first was a high-entropy quinary alloy, CrMnFeCoNi, and the second a medium-entropy quaternary alloy, CrFeCoNi. Both alloys had FCC crystal structures and were essentially single-phase with fully recrystallized microstructures and equiaxed grains containing numerous annealing twins suggestive of low stacking fault energies. Their tensile behavior was studied at temperatures in the range −196 °C to 1000 °C and at strain rates of 10^{-3} and 10^{-1} s^{-1}. Both alloys exhibited a strong temperature dependence of strength and weak strain-rate dependence. Temperature dependent strength is not usually seen in pure FCC metals but has been observed in several binary FCC solid solution alloys. What appears to be different in the present FCC high-entropy alloys is that the thermal part of the yield stress versus temperature curves extends to relatively high temperatures whereas, in FCC binaries, the transition from thermal to athermal behavior usually occurs at relatively low temperatures. These results imply that there may be stronger obstacles to dislocation motion in high-entropy alloys. However, further investigations are needed to understand the precise nature and distribution of these obstacles in the various alloys. The ductilities of both HE-1 and HE-4, instead of showing the typical inverse dependence on strength, increased in tandem with strength as the test temperature decreased from room temperature down to liquid nitrogen temperature: as the yield strengths doubled the elongations to fracture increased by a factor of 1.5 to values in excess of 60%. There was a high degree of work hardening evident at low temperatures, possibly due to deformation-induced nanoscale twinning. This likely postponed the onset of necking to higher strains and enhanced the ductility.

Acknowledgments

References

[1] Yeh JW, Chen SK, Lin SJ, Gan JY, Chin TS, Shun TT, et al. Nanostructured high-entropy alloys with multiple principal elements: novel alloy design concepts and outcomes. Adv Eng Mater 2004;6:299–303.

[2] Cantor B, Chang ITH, Knight P, Vincent AJB. Microstructural development in equiatomic multicomponent alloys. Mater Sci Eng A 2004;375-377:213–8.

[3] Yeh JW, Chen SK, Gan JY, Lin SJ, Chin TS, Shun TT, et al. Formation of simple crystal structures in Cu−Co−Ni−Cr−Al−Fe−Ti−V allaoys with multiprincipal metallic elements. Metall Mater Trans A 2004;35:2533–6.

[4] Huang PK, Yeh JW, Shun TT, Chen SK. Multi-principal-element alloys with improved oxidation and wear resistance for thermal spray coating. Adv Eng Mater 2004;6:74–8.

[5] Tong CJ, Chen YL, Chen SK, Yeh JW, Shun TT, Tsau CH, et al. Microstructure characterization of Al$_x$CoCrCuFeNi high-entropy alloy system with multi-principal elements. Metall Mater Trans A 2005;36:881–93.

[6] Tong CJ, Chen MR, Chen SK, Yeh JW, Shun TT, Tsau CH, et al. Mechanical performance of the Al$_x$CoCrCuFeNi high-entropy alloy system with multi-principal elements. Metall Mater Trans A 2005;36:1263–71.

[7] Yeh JW, Chen YL, Lin SJ, Chen SK. High-entropy alloys − a new era of exploitation. Mater Sci Forum 2007;560:1–9.

[8] Zhou YJ, Zhang Y, Wang YL, Chen GL. Solid solution alloys of AlCoCrFeNiTi$_x$ with excellent room-temperature mechanical properties. Appl Phys Lett 2007;90:181904.

[9] Wang XF, Zhang Y, Qiao Y, Chen GL. Novel microstructure and properties of multicomponent CoCrCuFeNiTi$_x$ alloys. Intermetallics 2007;15:357–62.

[10] Wang FJ, Zhang Y. Effect of Co addition on crystal structure and mechanical properties of Ti$_{0.5}$CrFeNiAlCo high entropy alloy. Mater Sci Eng A 2008;496:214–6.

[11] Shun TT, Hung CH, Lee CF. Formation of ordered/disordered nanoparticles in FCC high entropy alloys. J Alloys Compd 2010;493:105–9.

[12] Zhu JM, Fu HM, Zhang HF, Wang AM, Li H, Hu ZQ. Synthesis and properties of multiprincipal component AlCoCrFeNiSi$_x$ alloys. Mater Sci Eng A 2010;527:7210–4.

[13] Senkov ON, Wilks GB, Scott JM, Miracle DB. Mechanical properties of Nb$_{25}$Mo$_{25}$Ta$_{25}$W$_{25}$ and V$_{20}$Nb$_{20}$Mo$_{20}$Ta$_{20}$W$_{20}$ refractory high entropy alloys. Intermetallics 2011;19:698–706.

[14] Senkov ON, Scott JM, Senkova SV, Miracle DB, Woodward CF. Microstructure and room temperature properties of a high-entropy TaNbHfZrTi alloy. J Alloys Compd 2011;509:6043–8.

[15] Singh S, Wanderka N, Murty BS, Glatzel U, Banhart J. Decomposition in multicomponent AlCoCrCuFeNi high-entropy alloy. Acta Mater 2011;59:182–90.

[16] Lucas MS, Mauger L, Munoz JA, Xiao Y, Sheets AO, Semiatin SL, et al. Magnetic and vibrational properties of high-entropy alloys. J Appl Phys 2011;109:07E307.

[17] Lucas MS, Wilks GB, Mauger L, Munoz JA, Senkov ON, Michel E, et al. Absence of long-range chemical ordering in equimolar FeCoCrNi. Appl Phys Lett 2012;100:251907.

[18] Ng C, Guo S, Luan J, Shi S, Liu CT. Entropy-driven phase stability and slow diffusion kinetics in an Al$_{0.5}$CoCrCuFeNi high entropy alloy. Intermetallics 2012;31:165–72.

[19] Otto F, Yang Y, Bei H, George EP. Relative effects of enthalpy and entropy on the phase stability of equiatomic high-entropy alloys. Acta Mater 2013;61:2628–38.

[20] Liu WH, Wu Y, He JY, Nieh TG, Lu ZP. Grain growth and Hall-Petch relationship in a high-entropy FeCrNiCoMn alloy. Scripta Mater 2013;68:526–9.

[21] Carpenter HCH, Tamura S. Proc Roy Soc A 1926;113:161.

[22] Koppenaal TJ, Fine ME. Solid solution strengthening in alpha Cu-Al single crystals. Trans Metall Soc AIME 1962;224:347–53.

[23] Mitchell TE. Dislocations and plasticity in single crystals of face centered cubic metals and alloys. In: Stanford EG, et al., editors. Progress in applied materials research, vol. 6. London: Heywood and Co.; 1964. p. 119.

[24] Wigley DA. Mechanical properties of materials at low temperatures. New York: Plenum Press; 1971.

[25] Basinski ZS, Foxall RA, Pascual R. Stress equivalence of solution hardening. Scripta Mater 1972;6:807.

[26] Butt MZ, Feltham P. Solid-solution hardening. Acta Metall 1978;26:167–73.

[27] Traub H, Neuhäuser H. Ch. Schwink, Investigations of yield region of concentrated Cu−Ge and Cu−Zn single crystals. 1. Critical resolved shear-stress, slip line formation and true strain rate. Acta Metall 1977;25:437–46.

[28] Wille Th, Schwink Ch. Precision measurements of critical resolved shear-stress in CuMn alloys. Acta Metall 1986;34:1059–69.

[29] Wille Th, Gieseke W, Schwink Ch. Quantitative analysis of solution hardening in selected copper alloys. Acta Metall 1987;35:2679–93.

[30] Fleischer RL, Hibbard WR. "Solution hardening, " in the relation between structure and mechanical properties of metals. In: Proc. Conf. Held at the national physical laboratory, vol. 1. Middlesex: Teddington; 7−9 January 1963. p. 261.

[31] Otto F, Dlouhy A, Somsen Ch, Bei H, Eggeler G, George EP. Unpublished results. 2013.

[32] Thornton PR, Mitchell TE. Deformation twinning in alloys at low temperatures. Philos Mag 1962;7:361.

[33] Venables JA. Reed-Hill RE, Hirth JA, Rogers HC, editors. Deformation twinning. New York: Gordon Breach; 1963.